Coexisting chromian omphacite and diopside in tremolite schist from the Chugoku Mountains, SW Japan: The effect of Cr on the omphacite-diopside immiscibility gap

TATSUKI TSUJIMORI[1],* AND JUHN G. LIOU[2]

[1]Research Institute of Natural Sciences, Okayama University of Science, Okayama 700-0005, Japan
[2]Department of Geological and Environmental Sciences, Stanford University, Stanford, California 94305, U.S.A.

ABSTRACT

Chromian clinopyroxenes with exsolution textures were found in high-pressure (HP) tremolite schist from the Osayama serpentinite melange in the Chugoku Mountains, Southwestern Japan. Chromian omphacite [jadeite $(Jd)_{23.3-41.4}$ diopside $(Di)_{46.7-60.7}$ kosmochlor $(Ko)_{4.5-19.6}$ aegirine $(Ae)_{<7.0}$] with up to 6.6 wt% Cr_2O_3 occurs as neoblastic crystals in a foliated tremolite-rich matrix, or as pseudomorphs after relict chromian spinel, and contains irregular-shaped thin lamellae of chromian diopside $(Jd_{3.8-18.2}Di_{72.5-93.6}Ko_{1.1-13.9}Ae_{<3.4})$. Chromian omphacite contains roughly constant jadeite plus kosmochlor components at 38.2–51.6 mol%; this is equivalent to the jadeite component of ordered $P2/n$ omphacite. Systematic analyses of coexisting chromian pyroxenes yield a clear immiscibility gap between "omphacite" and "diopside." The compositional gap becomes much narrower with increasing Ko component; addition of only 10 mol% Ko component narrows the omphacite-diopside gap by an order of magnitude. Such an effect is similar to, but more effective than, the introduction of Fe^{3+} on the omphacite-diopside immiscibility gap.

Chromian pyroxenes replacing relict chromian spinel are associated with other chromian silicates including phengite, chlorite, and pumpellyite. The wide compositional gap of chromian pyroxenes and the presence of chromian pumpellyite and Si-rich chromian phengite indicate $T < 300–400$ °C and $P > 0.8$ GPa. This P-T estimate is consistent with parageneses of minerals in the host serpentinite. The variation of Cr content in chromian silicates reflects the extent of Cr ↔ Al substitution, and may be related to a chemical heterogeneity of the Cr-bearing fluid.

INTRODUCTION

Omphacite is a common metamorphic mineral in high-pressure (HP) - ultrahigh-pressure (UHP) metamorphic rocks. At $T < 500$ °C, an immiscibility gap between Fe^{3+}-poor omphacite and diopsidic pyroxene is well defined because of the difference in space-group symmetry between ordered ($P2/n$ symmetry) omphacite and disordered ($C2/c$ symmetry) diopsidic pyroxene (e.g., Carpenter 1980a; Carpenter et al. 1990). Coexisting Fe^{3+}-poor omphacite and diopsidic pyroxene (or augite) pairs have been reported from blueschist-facies rocks (e.g., Brown et al. 1978; Carpenter 1980a; Enami and Tokonami 1984; Tsujimori 1997). Moreover, a compositional gap between Fe^{3+}-poor omphacite and "chloromelanite" (in classic nomenclature by Essene and Fyfe 1967) has also been examined from natural occurrences (e.g., Maruyama and Liou 1987; Philippot and Kienast 1989). On the other hand, some omphacites in Cr-rich rocks contain significant kosmochlor $(NaCr^{3+}Si_2O_6)$ component due to Al ↔ Cr substitution (e.g., Nishiyama et al. 1986; Harlow and Olds 1987; Philippot and Kienast 1989; Liu et al. 1998). The effect of Cr on omphacite-diopside immiscibility is not known, because the coexistence of chromian omphacite and diopside is rare in natural parageneses.

Coexisting chromian pyroxenes were recently found in a tremolite schist from SW Japan. The chromian pyroxene pairs are associated with other chromian HP minerals (phengite, pumpellyite, and chlorite), and their compositions were analyzed; the

results yield a well-defined immiscibility gap between chromian omphacite and diopside. The compositional gap reported here provides the first evidence of omphacite-diopside immiscibility in the Cr-bearing system.

Geologic setting

The Osayama serpentinite melange in the central Chugoku Mountains (Fig. 1) contains tectonic blocks of Paleozoic lawsonite-blueschist to epidote-blueschist facies rocks (Tsujimori 1998). Phengite K-Ar ages from the HP schists are 273–327 Ma, and are concentrated around 320 Ma regardless of rock type and metamorphic grade (Tsujimori and Itaya 1999). The protoliths of the serpentinite are mainly harzburgite and minor cumulate dunite as indicated by relict igneous olivine, orthopyroxene, clinopyroxene, and chromian spinel. Rare winchitic to tremolitic amphiboles and diopside occur as metamorphic minerals in the serpentinite. Several occurrences of jadeitite and omphacitite have been identified (Kobayashi et al. 1987; Tsujimori 1997). Tsujimori (1997) described coexisting omphacite and diopside from an omphacitite. Late Cretaceous granitic intrusions caused thermal recrystallization of serpentinite in the western part of the area (Nozaka and Shibata 1995; Tsujimori 1998).

In the serpentinite melange, two types of tremolite-rich rocks occur: (1) tremolite schist of peridotite-origin; and (2) tremolite-rich rind at the boundaries between mafic schist blocks and serpentinite. The tremolite schist occurs as blocks and contains relict chromian spinel replaced by HP minerals such as high-Si phengite. The K-Ar age of chromian phengite is 354 Ma (Tsujimori, unpublished data). The investigated sample is a tremolite
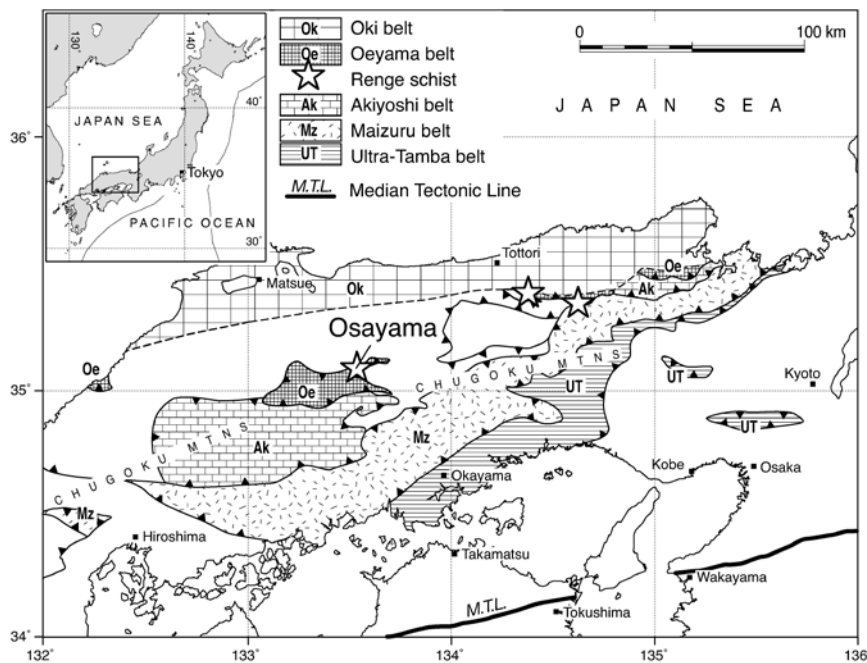
FIGURE 1. Simplified map of the Chugoku Mountains, showing various petrotectonic units and the sampling locality in the Osayama Mountain (modified after Tsujimori 2002).

schist. The tremolite-rich rind commonly lacks clinopyroxene. Talc and rare titanite occur as accessories. However, randomly oriented, neoblastic diopside and uvarovite-rich garnet commonly occur in the thermal aureole of Late Cretaceous granitic intrusions. Sakamoto and Takasu (1996) described kosmochlor-diopside series pyroxenes ($Jd_{0–8.9}Di_{45.3–97.5}Ae_{0–5.7}Ko_{0.1–54.0}$) from a tremolite-rich metasomatic rock adjacent to blueschist blocks. Similar chromian pyroxenes ($Jd_{3.2–7.3}Di_{54.9–94.0}Ae_{0–1.8}Ko_{0.5–39.1}$) occur as albite-uvarovite veins that fill cracks of tremolite-rich rocks (Tsujimori 1998). The textures and associated minerals suggest that these chromian pyroxenes may have formed locally from a Cr-rich fluid that was introduced from the adjacent serpentinite by hydrothermal events, probably related to the Late Cretaceous granitic intrusion.

Sample description

The investigated tremolite schist occurs as a small block (30×30 cm in size) in sheared serpentinite at an outcrop 2×2 m in width. In this outcrop, an omphacitite (30×30 cm in size) described by Tsujimori (1997) and a pumpellyite- and epidote-bearing blueschist occur (60×20 cm in size) as blocks in serpentinite.

The tremolite schist consists mostly of tremolite (>90%), with a small amount of omphacite and phengite. It has a well-developed penetrative foliation defined by preferred orientation of slender or acicular tremolite (<4 mm). Elongated, emerald-green seams, up to 10 mm in length, are scattered in a foliated matrix. The green seams typically preserve relict brownish chromian spinel, and are composed of phengite, omphacite, chlorite, pumpellyite, and garnet. In the green seams, relict brown spinel (<0.4 mm) is fractured and replaced by omphacite, phengite, and garnet.

Omphacite occurs as coronas surrounding relict spinel in the emerald-green seams (Figs. 2a and 2b) and as neoblasts (<0.3 mm in length) in the matrix. Chromian diopside occurs as irregular-shaped patches or as lamellae in chromian om-

phacite (Figs. 2c, 2d, 2e, and 2f). Some chromian omphacites contain inclusions of chromian phengite and rare K-feldspar (of $Or_{95–97}Ab_{3–5}$). Chromian phengite occurs in green seams as lepidoblasts or aggregates with striking green pleochroism. Chromian chlorite occurs as aggregates of small tabular crystals, whereas rare chromian pumpellyite appears as colorless prisms (<0.6 mm in length) with low birefringence. Chromian garnet is a secondary phase, as it occurs as irregularly shaped aggregates of fine-grained crystals and fills grain boundaries and cracks of chromian omphacite and phengite. Some chromian garnets replace relict chromian spinel.

MINERAL CHEMISTRY

Methods

Electron microprobe analysis was carried out with a JEOL JXA-8800R at Kanazawa University. Quantitative analyses of rock-forming minerals were performed with 15 kV accelerating voltage, 12 nA beam current, and 3–5 μm beam size. Natural and synthetic silicates and oxides were used for calibration. The ZAF method (oxide basis) was employed for matrix corrections. Overall compositional features of mafic minerals in the tremolite schists are illustrated on a Cr/(Cr + Al) vs. Mg/(Mg + Fe^{2+}) diagram (Fig. 3). Representative microprobe analyses of coexisting chromian clinopyroxene pairs and other minerals are presented in Tables 1 and 2, respectively.

Clinopyroxenes

The Fe^{2+}/Fe^{3+} ratio for clinopyroxene was estimated assuming a cation total of four. Although Cr may be accommodated in the clinopyroxene in structure as $NaCrSi_2O_6$ (kosmochlor) or $CaCrAlSiO_6$ (Cr-Tschermak's) components, the analyzed clinopyroxenes do not contain any Al in the tetrahedral site. Thus, the Cpx consists of only four end-members, jadeite (Jd), diopside (Di), aegirine (Ae), and kosmochlor (Ko); they were calculated as Jd = Al, Di = Ca, Ko = Cr, and Ae = Fe^{3+}, respectively, and normalized to Jd + Di + Ko + Ae = 100.
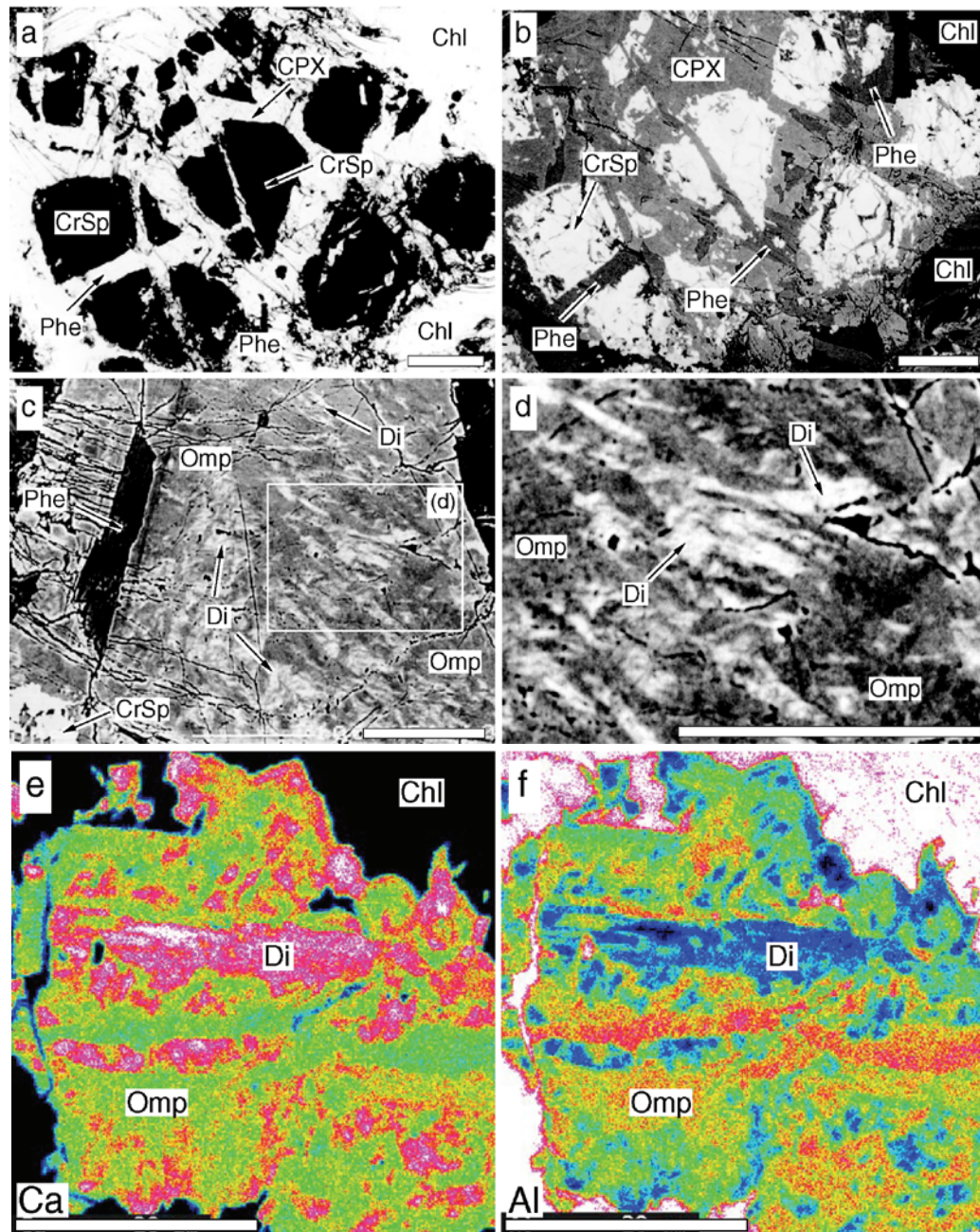
FIGURE 2. Photomicrograph showing occurrences and microtextures of chromian clinopyroxenes in the investigated tremolite schist. (**a**) Cross-polarized view showing chromian clinopyroxenes (CPX) replacing relict chromian spinel; Cr-bearing matrix minerals including chlorite and phengite are also shown. (**b**) Back-scattered electron image of same clinopyroxene grain of **a**. (**c**) Back-scattered electron image showing lamellae of chromian diopside in chromian omphacite. (**d**) Enlarged image of a part of chromian diopside lamellae in chromian omphacite. (**e**) X-ray image of Ca$K\alpha$ of coexisting chromian omphacite and diopside. (**f**) X-ray image of Al$K\alpha$ of **e**. Scale bars on each image represent 100 μm.

Omphacite contains 1.6–6.6 wt% Cr_2O_3, and has a composition of Jd = 23.3–41.4%, Di = 46.7–60.7%, Ko = 4.5–19.6%, and Ae < 7.0% (Fig. 4). The Mg/(Mg + Fe^{2+}) ratio ranges from 0.80 to 0.94 and the Cr/(Cr + Al) ratio varies from 0.10 to 0.45. Although the Cr content in omphacite is variable, even in a single discrete crystal and heterogeneous in a thin section, a few omphacite grains with higher Cr content occur nearby relict

chromian spinel. No systematic prograde or retrograde chemical zoning is observed in chromian omphacite. High-Cr omphacite tends to be in contact with Cr-richer diopside (Fig. 4).

Diopside lamellae contain 0.4–4.6 wt% Cr_2O_3, and have a composition of Jd = 3.8–18.2%, Di = 72.5–93.6%, Ko = 1.1–13.9%, and Ae < 3.4% (Fig. 4). The Mg/(Mg + Fe^{2+}) ratio ranges from 0.84 to 0.90. The Cr/(Cr + Al) ratio varies from 0.17 to 0.60.

TABLE 1. Representative electron-microprobe analyses of coexisting chromian pyroxene pairs. Omp = chromian omphacite; Di = chromian diopside

Pair	A		B		C		D		E	
	Omp	Di	Omp	Di	Omp	Di	Omp	Di	Omp	Di
SiO_2	56.89	55.58	56.83	55.40	56.19	55.11	56.97	55.84	56.97	55.27
TiO_2	0.20	0.01	0.06	0.00	0.06	0.01	0.08	0.07	0.08	0.02
Al_2O_3	8.42	1.08	9.73	1.74	7.96	4.24	9.11	3.82	9.11	2.06
Cr_2O_3	3.59	0.50	1.61	1.68	2.41	2.16	2.39	2.32	2.39	4.58
FeO*	2.97	3.62	3.00	3.89	3.60	3.89	3.18	3.86	3.18	3.16
MnO	0.11	0.27	0.05	0.19	0.19	0.23	0.04	0.11	0.04	0.23
MgO	8.31	15.09	8.82	13.74	8.87	11.77	8.85	12.34	8.85	12.36
CaO	12.96	23.45	13.13	21.43	14.20	18.60	13.06	18.12	13.06	18.59
Na_2O	7.27	1.15	7.21	2.10	6.39	3.87	7.08	3.90	7.08	3.55
K_2O	0.02	0.02	0.02	0.04	0.06	0.03	0.02	0.00	0.02	0.03
Total	100.74	100.77	100.46	100.21	99.93	99.91	100.78	100.38	100.78	99.85
(O=6)										
Si	2.018	2.014	2.005	2.019	2.014	1.999	2.012	2.014	2.012	2.020
Ti	0.005	0.000	0.002	0.000	0.002	0.000	0.002	0.002	0.002	0.001
Al	0.352	0.046	0.405	0.075	0.336	0.181	0.379	0.162	0.379	0.089
Cr	0.101	0.014	0.045	0.048	0.068	0.062	0.067	0.066	0.067	0.132
Fe^{3+}	0.002	0.000	0.032	0.000	0.011	0.032	0.012	0.013	0.012	0.000
Fe^{2+}	0.086	0.117	0.057	0.129	0.097	0.086	0.081	0.103	0.081	0.106
Mn	0.003	0.008	0.001	0.006	0.006	0.007	0.001	0.003	0.001	0.007
Mg	0.439	0.815	0.464	0.747	0.474	0.636	0.466	0.663	0.466	0.674
Ca	0.492	0.910	0.496	0.837	0.545	0.723	0.494	0.700	0.494	0.728
Na	0.500	0.081	0.493	0.148	0.444	0.272	0.485	0.273	0.485	0.252
K	0.001	0.001	0.001	0.002	0.003	0.001	0.001	0.000	0.001	0.001
Cr'	0.22	0.24	0.10	0.39	0.17	0.25	0.15	0.29	0.15	0.60
Mg'	0.84	0.87	0.89	0.85	0.83	0.88	0.85	0.87	0.85	0.86
Jd	37.2	4.8	41.4	7.8	35.0	18.2	39.8	17.2	39.8	9.4
Ae	0.2	0.0	3.2	0.0	1.1	3.2	1.3	1.4	1.3	0.0
Di	52.0	93.8	50.8	87.2	56.8	72.4	51.9	74.4	51.9	76.7
Ko	10.6	1.5	4.6	5.0	7.1	6.2	7.0	7.0	7.0	13.9
Jd+Ko	47.8	6.2	46.0	12.8	42.1	24.4	46.8	24.3	46.8	23.3

Note: FeO* = total Fe as FeO. Cr' = Cr/(Cr + Al). Mg' = Mg/(Mg + Fe²⁺)

TABLE 2. Representative electron-microprobe analyses of tremolite, relict chromian spinel, and chromian silicates

	Tremolite		Cr-Spinel		Phengite		Pumpellyite		Chlorite		Garnet (2nd)	
					Core	Rim						
SiO_2	58.38	58.26	0.02	0.33	52.98	52.52	36.94	37.91	30.32	30.34	37.81	37.88
TiO_2	0.05	0.01	0.00	0.09	0.00	0.00	0.09	0.06	0.00	0.00	0.31	0.28
Al_2O_3	0.50	0.33	22.94	19.41	22.73	23.85	18.49	23.02	17.92	18.06	11.25	12.34
Cr_2O_3	0.64	0.03	41.62	40.16	4.95	4.04	10.93	4.30	3.26	2.48	12.69	11.12
FeO*	3.76	4.37	23.99	30.96	1.56	1.36	1.31	1.26	9.95	10.17	2.30	2.71
MnO	0.12	0.09	0.68	2.36	0.09	0.01	0.34	0.30	0.19	0.10	1.39	1.02
MgO	21.44	21.80	10.47	1.00	4.45	4.51	3.51	3.77	26.05	25.40	0.03	0.09
CaO	12.25	12.73	0.00	0.13	0.01	0.01	21.34	22.16	0.08	0.07	33.51	34.30
Na_2O	0.80	0.52			0.20	0.13	0.38	0.24	0.00	0.00	0.00	0.01
K_2O	0.12	0.12			10.40	10.61	0.01	0.03	0.00	0.02	0.00	0.04
NiO			0.01	0.06								
ZnO			0.24	5.16								
Total	98.06	98.26	99.72	99.66	97.37	97.04	93.34	93.05	87.77	86.64	99.29	99.79
O=	23	23	4	4	22	22	24.5	24.5	28	28	12	12
Si	8.010	7.980	0.001	0.011	6.986	6.929	6.053	6.085	5.912	5.979	3.013	2.986
Ti	0.005	0.001	0.000	0.002	0.000	0.000	0.011	0.008	0.000	0.000	0.019	0.017
Al	0.080	0.053	0.841	0.775	3.532	3.709	3.572	4.355	4.118	4.195	1.056	1.146
Cr	0.069	0.004	1.024	1.076	0.516	0.421	1.416		0.546	0.503	0.386	0.799	0.693
Fe3+	0.000	0.084	0.134	0.130					0.080	0.161		
Fe2+	0.431	0.416	0.490	0.747	0.172	0.150	0.180	0.169	1.624	1.676	0.073	0.018
Mn	0.014	0.010	0.018	0.068	0.010	0.001	0.047	0.041	0.031	0.017	0.094	0.068
Mg	4.385	4.451	0.486	0.050	0.874	0.886	0.858	0.902	7.571	7.460	0.004	0.011
Ca	1.800	1.868	0.000	0.009	0.001	0.001	3.747	3.811	0.017	0.014	2.861	2.896
Na	0.212	0.139			0.050	0.033	0.120	0.074	0.002	0.001	0.000	0.001
K	0.021	0.022			1.750	1.786	0.002	0.006	0.001	0.006	0.000	0.004
Ni			0.000	0.002								
Zn			0.006	0.129								
Total	15.027	15.029	3.000	3.000	13.890	13.916	16.004	15.997	19.779	19.734	8.000	8.000
Cr'	0.46	0.06	0.55	0.58	0.13	0.10	0.28	0.11	0.11	0.08	0.43	0.38
Mg'	0.91	0.91	0.50	0.06	0.84	0.86	0.83	0.84	0.82	0.82	0.05	0.38

Notes: FeO* = total Fe as FeO. Cr' = Cr/(Cr+Al). Mg' = Mg/(Mg + Fe²⁺).
Fe³⁺/Fe²⁺ ratios are estimated with total cation = 3 for Cr-spinel, total cation = 8 for garnet, and total cation = 13 exclusive of Ca, Na, and K (O = 23) for tremolite.
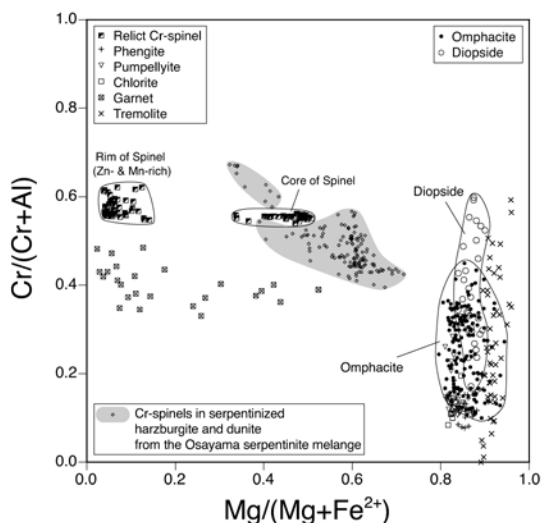
FIGURE 3. $Cr/(Cr + Al)$ vs. $Mg/(Mg + Fe^{2+})$ diagram showing overall compositional features of analyzed mafic minerals in the tremolite schists. Relict chromian spinels in serpentinized harzburgite and dunite from the Osayama serpentinite melange are also plotted.

Other minerals in emerald-green seams

Relict spinel shows distinct chemical zoning. The core may represent the primary relict igneous composition and was replaced by rim composition along cracks and crystal margins (Fig. 3). The core is characterized by a high $Mg/(Mg + Fe^{2+})$ ratio (0.34–0.51), low ZnO (0.06–0.56 wt%), and MnO (0.47-1.36 wt%); the $Cr/(Cr+Al)$ ratio is 0.54-0.56. On the other hand, the rim is enriched in ZnO (1.2–6.6 wt%) and MnO (1.8–2.6 wt%), and is characterized by a remarkably low $Mg/(Mg + Fe^{2+})$ ratio (0.04–0.14); the $Cr/(Cr + Al)$ ratio varies from 0.55 to 0.62. The $Cr/(Cr + Al)$ and $Mg/(Mg + Fe^{2+})$ ratios of the core are similar to those from serpentinized harzburgite and dunite of melange-matrix reported by Tsujimori (1998) (Fig. 3).

Phengite contains 3.0–7.4 wt% Cr_2O_3 and appreciable amounts of celadonite component with Si p.f.u. = 6.8–7.0 (O = 22). The $Mg/(Mg + Fe^{2+})$ ratio is 0.81–0.88. The $Cr/(Cr + Al)$ ratio varies from 0.08 to 0.19.

Pumpellyite contains 4.1–10.9 wt% Cr_2O_3, with an $Mg/(Mg + Fe)$ ratio of 0.81–0.86 and a $Cr/(Cr + Al)$ ratio of 0.11 to 0.28. The $(Al + Cr)/(Al + Cr + Fe + Mg)$ ratio of this phase is about 0.8, which is similar to the $Al/(Al + Fe + Mg)$ ratio of Cr-free pumpellyites from other blueschist facies rocks at Osayama.

Chlorite is clinochlore containing 2.5–5.2 wt% Cr_2O_3. The $Mg/(Mg + Fe^{2+})$ ratio ranges from 0.81 to 0.86, and the $Cr/(Cr + Al)$ ratio is 0.08–0.20. The Si content is 5.8–6.1 pfu based on a formula with 28 O atoms.

Secondary garnet is enriched in grossular and uvarovite components with variable amounts of andradite, almandine, pyrope, and spessartine components ($Grs_{61.3–70.7}Uvr_{20.3–19.5}Adr_{1.9–6.0}Pyr_{0.1–2.2}Alm_{0.3–4.5}Sps_{1.8–3.4}$). It contains 10.0–14.1 wt% Cr_2O_3. The $Mg/(Mg + Fe^{2+})$ ratio varies extensively from 0.02 to 0.52, and the $Cr/(Cr + Al)$ ratio is 0.33–0.49.

As clearly shown in Figure 5, the negative correlation between Al and Cr in overall chromian silicates is due to a substitution of Cr for Al in octahedral site.
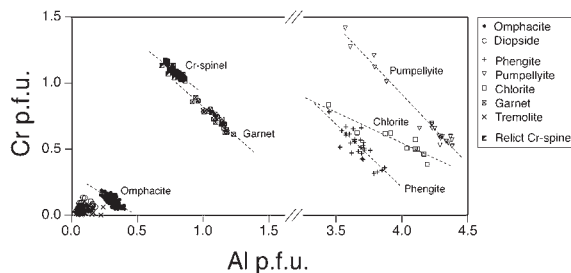
FIGURE 4. Composition of Cr-bearing clinopyroxenes on the Ko-Jd-Di ternary diagram. (**a**) Tremolite schist from the Osayama Mountain (the present study). Tie-lines connecting compositions of coexisting Cpx phases are shown. (**b**) Compositions of the other Cr-bearing omphacitic pyroxenes in literatures (1 = Nishiyama et al. 1986; 2 = Harlow and Olds 1987; 3 = Philippot and Kienast 1989; 4 = Liu et al. 1998; 5 = Sobolev et al. 1975). Hatched areas mean the compositional filed of two Cr-bearing pyroxenes plotted in **a**.
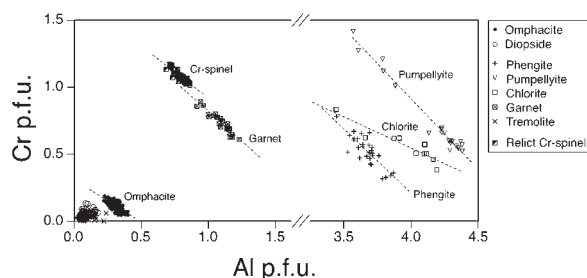
FIGURE 5. Cr vs. Al diagram showing the Cr ↔ Al substitution of analyzed Cr-bearing minerals. The amounts of Cr and Al for these phases are calculated based on their appropriate structural formulae.

Matrix tremolite

Tremolite in the matrix contains less than 1.0 wt% Cr_2O_3 and Na_2O. The $Mg/(Mg + Fe^{2+})$ and the $Cr/(Cr + Al)$ ratios range respectively from 0.89 to 0.96 and from 0 to 0.59.

Petrogenesis

The metamorphic *P-T* condition for the tremolite schist is estimated based on available phase equilibira. The presence of chromian pumpellyite and absence of epidote suggest that the maximum temperature of metamorphism is limited by the following reaction:

Mg-Al pumpellyite = clinozoisite + grossular + chlorite + quartz + H_2O (Schiffman and Liou 1980).

Mevel and Kienast (1980) maintained that the Cr ↔ Al substitution of pumpellyite does not affect its *P*- and *T*- stability range. According to these results, the temperature of metamorphism was less than 400 °C at 0.9 GPa. The high Si content (7.0 p.f.u. for O = 22) of chromian phengite yields a minimum *P* = 0.8–0.9 GPa at a nominal *T* = 300 °C (Massonne and Schreyer 1987). Furthermore, the omphacite-kosmochlor solid-solution may suggest a HP environment, because omphacite itself is an index mineral for HP metamorphism.

The presence of two coexisting pyroxenes also may provide constraints on the temperature of metamorphism. Two different possible phase relations between omphacite and diopside have

been proposed. Carpenter (1980b) suggested phase relations in the jadeite-diopside system in which the apparent consolute temperature for the miscibility gap between ordered omphacite (*P2/n*) and diopside (*C2/c*) is about 500 °C. He proposed a second-order transformation mechanism for the *C2/c* ↔ *P2/n* transition. On the other hand, Enami and Tokonami (1984) proposed a first-order transformation model for the transformation *C2/c* to *P2/n* to explain the persistence of some disordered omphacites (*C2/c*). The solvus between the ordered omphacite (*P2/n*) and diopside (*C2/c*) becomes wider with decreasing temperature in both cases. The wide compositional gap (Jd_8-Jd_{41}) among Cr-poor pairs indicates a low-*T* environment (*T* < 300 °C) (Carpenter 1980b). In these previous studies, the effect of Cr on the transformation temperature and immiscibility gap was not discussed.

In some HP metamorphic rocks, chromian silicates occur around relict or detrital chromian spinel (e.g., Harlow and Olds 1987; Gil Ibarguchi et al. 1991; Banno 1993). Chromian silicates were suggested to have formed through reactions involving partial destruction of chromian spinel by hydrothermal fluids during metamorphism. Harlow and Olds (1987) mentioned that the

Cr/(Cr + Al) ratio of chromian silicates is always less than that of relict chromian spinel; similar results are shown in Figure 3 for most of our investigated samples. This feature suggests that maximum Cr solubility in chromian silicates, i.e., the degree of the Cr ↔ Al substitution, is highly dependent on the Cr/(Cr + Al) ratio of the original spinel composition. On the other hand, a significant feature of our sample is that the chromian clinopyroxenes occur in both of the green seams with relict chromian spinel, and in the matrix in which neither relict spinel nor its pseudomorph are found. The presence of matrix Cr-rich pyroxenes suggests the mobilization of Cr under HP metamorphism, possibly by transport in an alkali solution. Although generally regarded as relatively immobile during metamorphism, the mobility of Cr during the alteration or metamorphism of ultramafic rocks has been pointed out by several authors (e.g., Nishiyama et al. 1986; Kerrich et al. 1987; Philippot and Kienast 1989). Serpentinite-related, alkali-rich fluids may play an important role in the mobilization of Cr during the metasomatic alteration of ultramafic rocks. The heterogeneity of Cr content in chromian silicates may be related to a chemical heterogeneity of local fluid compositions. As mentioned above, the diopside shows the
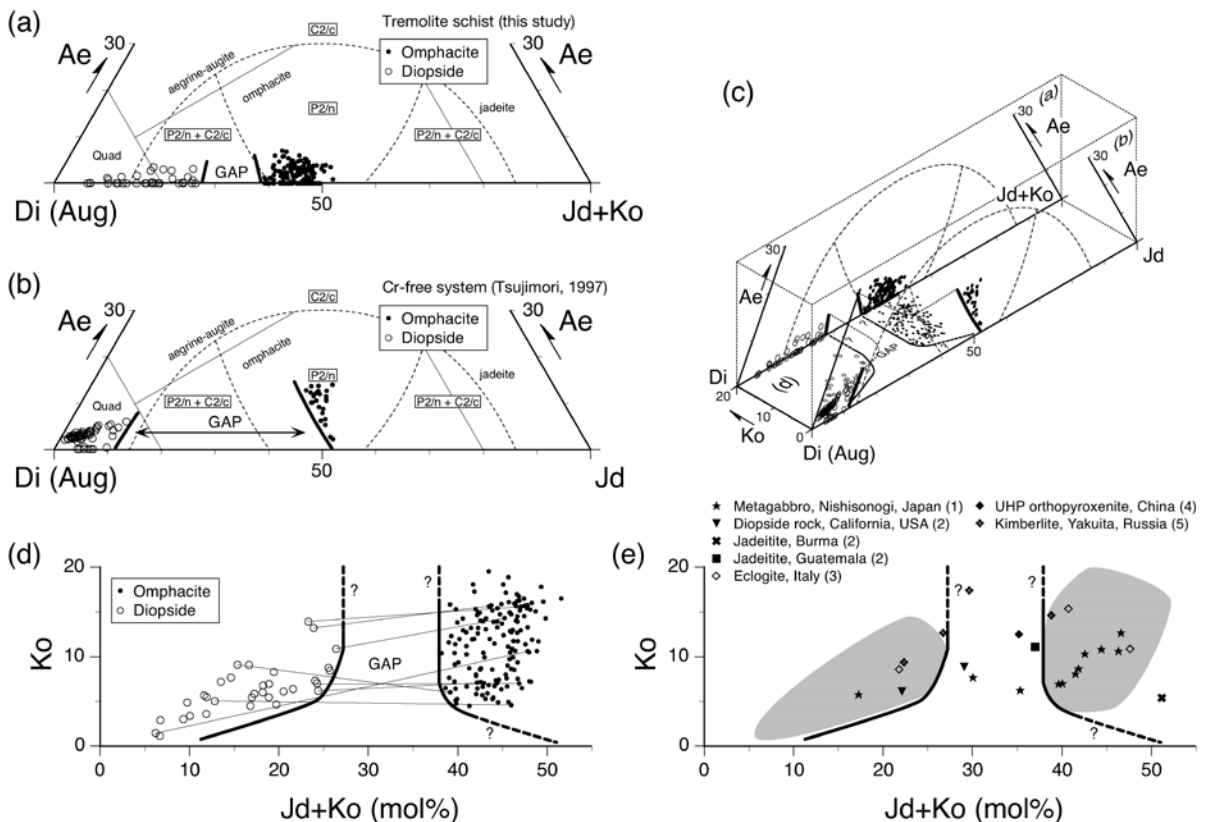
FIGURE 6. Compositional plots of analyzed omphacite and diopside showing the effect of the Ko component on the immiscibility between omphacite and diopside. (**a**) Compositions of two Cr-bearing clinopyroxenes on the (Jd + Ko)-Di-Ae ternary diagram. The apparent compositional gap is shown as bold lines. Phase relations in the Jd-Di-Ae system proposed by Carpenter (1980b) are also shown as dashed lines. (**b**) Compositions of coexisting Cr-free omphacite and diopside (augite) from the same outcrop by Tsujimori (1997; additional data) on the Jd-Di-Ae diagram. The compositional gap is shown as bold lines. (**c**) The three-dimensional illustration showing tentative phase relation between Cr-bearing and Cr-free systems at the same *P-T* condition. (**d**) Compositions of two Cr-bearing clinopyroxenes (the present study) on the Ko-(Jd + Ko) diagram. (**e**) Compositions of the other Cr-bearing omphacitic pyroxenes in literatures (1 = Nishiyama et al. 1986; 2 = Harlow and Olds 1987; 3 = Philippot and Kienast 1989; 4 = Liu et al. 1998; 5 = Sobolev et al. 1975). Hatched areas mean the compositional filed of two Cr-bearing pyroxenes plotted in **d**.

lamellar texture. This texture suggests that a continuous solid solution between diopside and omphacite exists under blueschist-facies conditions, and the diopside lamellae have exsolved from omphacite during retrogression.

In the green seams, relict spinel has a Zn- and Mn-enriched rim with a low $Mg/(Mg + Fe^{2+})$ ratio. The low $Mg/(Mg + Fe^{2+})$ ratio may be related to cation redistribution between original spinel and newly formed mafic minerals at low-T conditions. The increase of Zn and Mn in the rim may have resulted from a metasomatic process to form HP chromian silicates under blueschist-facies conditions. The core compositions of relict spinel corresponds to the compositions of primary chromian spinel in serpentinized peridotites (Fig. 3). Thus, the tremolite schist is the product of blueschist-facies metamorphism of serpentinized peridotite at $T < 300$–400 °C and $P > 0.8$ GPa, and Cr-bearing silicates were formed by metasomatic reaction between relict chromian spinel and Ca- and alkali-rich hydrothermal fluids.

Effect of Cr on the omphacite-diopside immiscibility

The omphacite of our investigated samples contains variable amounts of Cr, ranging from 1.6 to 6.6 wt% Cr_2O_3 even at the thin section scale. However, the sum of jadeite and kosmochlor components falls in a narrow range of 38.2–51.6 mol% and is equivalent to the jadeite component of the ordered $P2/n$ omphacite (Carpenter 1980b). In other words, the Ko component behaves itself like a Jd component in the structural formula in chromian omphacite. A similar feature was pointed out on chromian jadeite from Western Alps (Mevel and Kienast 1980).

To evaluate the effect of Cr on the omphacite-diopside immiscibility gap, the coexisting Cr-free omphacite and diopside in omphacitite described by Tsujimori (1997) is illustrated in Figure 6b. A wide composition gap is shown as diopside contains less than 10 mol% Jd whereas the omphacite ranges from 52 to 48 mol% Jd. As mentioned above, these Cr-free pyroxenes were found at the same outcrop and also coexist with pumpellyite suggesting that the tremolite schist and omphacitite experienced same P-T conditions within the pumpellyite-stability field. If we compare the Cr-bearing and Cr-free systems shown in Figure 6c, the apparent gap between omphacite and diopside becomes considerably narrower in the Cr-bearing system. This feature is apparent when the analysed chromian clinopyroxenes are plotted on the Ko vs. Jd + Ko diagram of Figure 6d. As shown in Figure 6d, the compositional gap is nearly constant for Cpx with more than 10 mol% Ko; at lower Ko, diopsidic pyroxenes increase Jd + Ko content with increasing Ko whereas the coexisting omphacites appear to have opposite relations. The solubility of only 10 mol% Ko component in the omphacite solid-solution significantly narrows the omphacite-diopside gap.

Thus far, several experimental studies have been performed on the effect of the kosmochlor component on Cpx solid-solution. The immiscibility gap in the diopside-kosmochlor system at anhydrous conditions ($Di_{76}Ko_{24}$-Ko_{100}) was found at 900–1450 °C and one atmospheric pressure by Ikeda and Yagi (1972), and the gap becomes narrower with increasing pressure ($Di_{80}Ko_{20}$-$Di_{55}Ko_{45}$: 1.5 GPa, 900–1450 °C (Ikeda and Ohashi 1977). Vredevoogd and Forbes (1975) showed that the solubility of

kosmochlor in diopside decreases with increasing pressure. These results are in contrast with the suggestion of complete solid-solution between diopside and kosmochlor under hydrous conditions (200 MPa, 700 °C) by Yoder and Kurellud (1971). Moreover, a complete solid solution between jadeite and kosmochlor exists at pressures greater than 1.8 GPa at 800 °C, whereas only kosmochlor-rich clinopyroxenes ($>Ko_{86}$) are stable at LP (0.1 MPa) (Abs-Wurmbach and Neuhaus 1976).

There is no experimental work on the solubility of Cr in omphacite; however, Cr-bearing omphacite has been documented in several HP/UHP rocks. Discrete crystals of omphacite in epidote-blueschist facies metagabbro at Nishisonogi (Japan) contain up to 4.1 wt% Cr_2O_3 (Nishiyama et al. 1986). Omphacite cores within otherwise Cr-free omphacite and inclusions in garnet of eclogite-facies vein from the Western Alps (Italy) have up to 8.9 wt% Cr_2O_3 (Philippot and Kienast 1989). Omphacites from Brumese and Guatemalan jadeitites and California omphacite have up to 4.1 wt% Cr_2O_3 (Harlow and Olds 1987). These occurrences do not exhibit exsolution textures; some analyses of these omphacites lie in the compositional gap described above (Fig. 6e). However, it should be emphasized that omphacites at Nishisonogi with a wide compositional range that overlaps with our compositional gap (Nishiyama et al. 1986) coexist with epidote; lack of pumpellyite or lawsonite-bearing assemblage in the Nishisonogi area suggests a relatively higher T than the investigated area. This relation suggests that the gap closes in the epidote-stability range. Moreover, disordered ($C2/c$) chromian omphacitic pyroxenes (avg. $Jd_{13.5}Di_{60.2}Ko_{24.8}Ae_{0.7}CaTs_{0.8}$) from UHP orthopyroxenite (1025 °C at 3 GPa) from the Dabie Mountains, central China (Liu et al. 1998), and chromian omphacites from diamond-bearing kimberlite from Yakuita (Sobolev et al. 1975) have compositions between our omphacite and diopside. It seems that the exsolution feature of chromian omphacite in natural occurrences (Figs. 5b and 6e) is limited to very low-T conditions <300–400 °C.

By analogy with the immiscibility gap between the disordered omphacite ($P2/n$) and the disordered pyroxenes in the jadeite-diopside-aegirine system (Carpenter 1980b), a miscibility gap between disordered omphacite ($P2/n$) and jadeite ($C2/c$), or kosmochlor ($C2/c$) would be expected. In fact, the presence of disordered ($C2/c$) chromian omphacitic pyroxenes under UHP condition (Liu et al. 1998) implies an analogy between the jadeite-diopside-aegirine and the jadeite-diopside-kosmochlor system. Carpenter (1980b) suggested that the addition of Fe^{3+} (aegirine component) enlarges the stability field of the $P2/n$ omphacite, and narrows the immiscibility range. The addition of Cr for the omphacite-diopside may have a similar but more profound effect. Such a difference may be due to the differences in the ratio of ionic radii of Al to Fe^{3+} (2%) and Cr^{3+} (14%) (Shannon 1976). Nevertheless, the similar effect also suggests that the compositional gap in the Cr-bearing system is limited to very low-T conditions.

REFERENCES CITED

Abs-Wurmbach, I. and Neuhaus, A. (1976) The system NaAlSi$_2$O$_6$ (jadeite)-NaCrSi$_2$O$_6$ (Kosmochlor) in the pressure range 1 bar to 25 kbar at 800°C. Neues Jahrbuch fur Mineralogie Abhandlung, 127, 213–241.

Banno, Y. (1993) Chromian sodic pyroxene, phengite and allanite from the Sanbagawa blueschists in the eastern Kii Peninsula, central Japan. Mineralogical Journal, 16, 306–317.

Brown, P., Essene, E.J., and Peacor, D.R. (1978) The mineralogy and petrology of manganese-rich rocks from St. Marcel, Piedmont, Italy. Contributions to Mineralogy and Petrology, 67, 227–232.

Carpenter, M.A. (1980a) Mechanisms of exsolution in sodic pyroxenes. American Mineralogist, 64, 102–108.

———(1980b) Composition and cation order variations in a sector-zoned blueschist pyroxene. Contributions to Mineralogy and Petrology, 71, 289–300.

Carpenter, M.A., Domeneghetti, M-.C., and Tazzoli, V. (1990) Application of Landau theory to cation ordering in omphacite I: Equilibrium behavior. European Journal of Mineralogy, 2, 7–18.

Enami, M. and Tokonami, M. (1984) Coexisting sodic diopside and omphacite in a Sanbagawa metamorphic rocks, Japan. Contributions to Mineralogy and Petrology, 86, 241–247.

Essene, E.J. and Fyfe, S. (1967) Omphacite in Californian metamorphic rocks. Contributions to Mineralogy and Petrology, 15, 1–23.

Gil Ibarguchi J.I., Mendia, M., and Girardeau, J. (1991) Mg- and Cr-rich staurolite and Cr-rich kyanite in high-pressure ultrabasic rocks (Cabo Ortegal, northwestern Spain). American Mineralogist, 76, 501–511.

Harlow, G.E. and Olds, E.P. (1987) Observations on terrestrial ureyite and ureyitic pyroxene. American Mineralogist, 72, 126–136.

Ikeda, K. and Yagi, K. (1972) Synthesis of kosmochlor and phase equilibria in the join CaMgSi$_2$O$_6$ -NaCrSi$_2$O$_6$. Contributions to Mineralogy and Petrology, 36, 63–72.

Ikeda, K. and Ohashi, H. (1977) Crystal field spectra of diopside-kosmochlor solid solutions formed 15 kbar pressure. Journal of the Japanese Association of Mineralogists, Petrologists and Economic Geologists, 69, 103–109.

Kerrich, R., Fyfe, W.S., Barnett, R.L., Blair, B.B., and Willmore, L.M. (1987) Corundum, Cr-muscovite rocks at O'Briens, Zimbabwe: the conjunction of hydrothermal desilication and LIL-element enrichment-geochemical and isotopic evidence. Contributions to Mineralogy and Petrology, 95, 481–498.

Kobayashi, S., Miyake, H., and Shoji, T. (1987) A jadeite rock from Oosa-cho, Okayama Prefecture, Southwestern Japan. Mineralogical Journal, 13, 314–327.

Liu, X., Zhou, H., Ma, Z., and Chang, L. (1998) Chrome-rich clinopyroxene in orthopyroxeneite from Maowu, Dabie Mountains, central China: A second record and its implications for petrogenesis. The Island Arc, 7, 135–141.

Maruyama, S. and Liou, J.G. (1987) Clinopyroxene-a mineral telescoped through the processes of blueschist facies metamorphism. Journal of Metamorphic Geology, 5, 529–552.

Massonne, H.J. and Schreyer, W. (1987) Phengite geobarometry based on the limiting assemblage with K-feldspar, phlogopite and quartz. Contributions to Mineralogy and Petrology, 96, 212–224.

Mevel, C. and Kienast, J.R. (1980) Chromian jadeite, phengite, pumpellyite, and lawsonite in a high-pressure metamorphosed gabbro from the French Alps. Mineralogical Magazine, 47, 359–364.

Nishiyama, T., Uehara, S., and Shinno, I. (1986) Chromian omphacite from low-grade metamorphic rocks, Nishisonogi, Kyushu, Japan. Journal of Metamorphic Geology, 4, 69–77.

Nozaka, T. and Shibata, T. (1995) Mineral paragenesis in thermally metamorphosed serpentinites, Ohsa-yama, Okayama Prefecture. Earth Science Report of Okayama University, 2, 1–12.

Philippot, P. and Kienast, J.R. (1989) Chemical-microstructural changes in eclogites in eclogite-facies shear zones (Monviso, Western Alps, north Italy) as indicators of strain history and the mechanism and scale of mass transfer. Lithos, 23, 179–200.

Sakamoto, S. and Takasu, A. (1996) Kosmochlor from the Osayama ultramafic body in the Sangun metamorphic belt, southwest Japan. Journal of Geological Society of Japan, 102, 49–52.

Schiffman, P. and Liou J.G. (1980) Synthesis and stability relations of Mg-Al pumpellyite, Ca$_4$Al$_5$MgSi$_6$O$_{21}$(OH)$_7$. Journal of Petrology, 95, 217–225.

Shannon, R.D. (1976) Revised effective ionic radii and systematic studies of interatomic distances in halides and chalcogenides. Acta Crystallographica, A32, 751–767.

Sobolev, V.S., Sobolev, N.V., and Lavrent'ev, Yu.G. (1975) Chrome-rich clinopyroxenes from the kimberlites of Yakuita. Neues Jahrbuch fur Mineralogie Abhandlung, 123, 213–218.

Tsujimori, T. (1997) Omphacite-diopside vein in an omphacitite block from the Osayama serpentinite melange, Sangun-Renge metamorphic belt, southwestern Japan. Mineralogical Magazine, 61, 845–852.

——— (1998) Geology of the Osayama serpentinite melange in the central Chugoku Mountains, southwestern Japan: 320 Ma blueschist-bearing serpentinite melange beneath the Oeyama ophiolite. Journal of Geological Society of Japan, 104, 213–231. (in Japanese with English abstract)

——— (2002) Prograde and retrograde P-T paths of the Late Paleozoic glaucophane eclogite from the Renge metamorphic belt, Hida Mountains, southwestern Japan. International Geology Review, 44, 797–818.

Tsujimori, T. and Itaya, T. (1999) Blueschist-facies metamorphism during Paleozoic orogeny in southwestern Japan: phengite K-Ar ages of blueschist-facies tectonic blocks in a serpentinite m_lange beneath Early Paleozoic Oeyama ophiolite. The Island Arc, 8, 190–205.

Vredevoogd, J.J. and Forbes, W.C. (1975) The system diopside-ureyite at 20 kbar. Contributions to Mineralogy and Petrology, 52, 147–156.

Yoder, H.S. and Kurellud, G. (1971) Kosmochlor and the chromite-plagioclase association. Carnegie Institution of Washington Geophysical Laboratory, Annual Report, 69, 155–157

Errata

Novel phase transition in orthoenstatite by Jennifer M. Jackson, Stanislav V. Sinogeikin, Michael A. Carpenter, and Jay D. Bass (vol. 89, p. 239–244, 2004).

A file error occurred during the printing process which inserted font errors into Equation 1, some text after Equation 1, and Equation 5. The correction is below; and the web site has been corrected. *American Mineralogist* regrets this error.

on page 242:

The Landau free energy expansion for this transition has the form:

$$G = \frac{1}{2}a(T - T_c)Q^2 + \frac{1}{4}bQ^4 + \frac{1}{6}cQ^6 + \lambda_1 e_1 Q^2 + \lambda_2 e_2 Q^2 + \lambda_3 e_3 Q^2$$
$$+ \lambda_4 e_4^2 Q^2 + \lambda_5 e_5^2 Q^2 + \lambda_6 e_6^2 Q^2 + \frac{1}{2}\sum_{i,k=1-3} C_{ik}^o e_i e_k + \frac{1}{2}\sum_{i=4-6} C_{ii}^o e_i^2 \quad (1)$$

where Q is the order parameter, T_c is the critical temperature, a, b, and c are normal Landau coefficients, λ_1-λ_6 are coupling coefficients, e_1-e_6 are strains ($e_1 \neq e_2 \neq e_3 \neq 0$, $e_4 = e_5 = e_6 = 0$), and C_{ik}^0 are elastic constants of the *Cmca* structure.

further down page 242:

The variation of C_{33} is derived from the usual relationship (Slonsczewski and Thomas 1970):

$$C_{ik} = C_{ik}^o - \sum_{m,n} \frac{\partial^2 G}{\partial e_i \partial Q_m} \left(\frac{\partial^2 G}{\partial Q_m \partial Q_n} \right)^{-1} \frac{\partial^2 G}{\partial e_k \partial Q_n} \quad (5)$$

Coexisting chromian omphacite and diopside in tremolite schist from the chugoku Mountains, SW Japan: The effect of Cr on the omphacite-diopside immiscibility gap by T. Tsujimoi and J.G. Liou (vol. 89, pages 7–14, 2004).

Figure 4 on page 11 is the wrong version. Below is the correct version. The editors regret the error.